

Short Communication

Thunderstorm-associated responses in the vertical motion of the mid-latitude F-region ionosphere

V.V. Kumar^{a,*}, M.L. Parkinson^{a,1,2}, P.L. Dyson^{a,3}, G.B. Burns^{b,4}^a Department of Physics, La Trobe University, Melbourne, Victoria 3086, Australia^b Australian Antarctic Division, Australian Government, Kingston 7050, Australia

ARTICLE INFO

Article history:

Received 21 July 2008

Received in revised form

4 March 2009

Accepted 25 March 2009

Available online 5 April 2009

Keywords:

Mid-latitude ionosphere

Thunderstorm-ionosphere coupling

Superposed epoch analysis

ABSTRACT

Mid-latitude Digisonde Doppler velocities, auroral electrojet (AE) indices and cloud-to-ground (CG) lightning strokes during August 2003–2004 were used to study the perturbations in the F-region vertical drift associated with terrestrial thunderstorms. A superposed epoch analysis (SEA) showed that the F-region vertical drifts V_z had a net descent of $\sim 0.6 \text{ m s}^{-1}$ peaking $\sim 3 \text{ h}$ after lightning. Stronger downward perturbations of up to $\sim 0.9 \text{ m s}^{-1}$ were observed in the afternoon on the day prior to lightning days. The perturbations were less significant on the day after and insignificant during the remaining intervals up to 144 h on either side of the lightning. The stronger responses on the day before are consistent with causality because the lightning times were merely proxies for the physical mechanisms involved. The actual causes are unclear, but we discuss the possible roles of lightning-induced ionisation enhancements, intense electric fields penetrating upward from electrified clouds, and atmospheric gravity waves (AGWs) radiated from thunderstorms or from the accompanying tropospheric fronts. There is no doubt that the behaviour of the mid-latitude F-region is controlled by the thermospheric winds and the solar wind-magnetosphere electrical generators, but our results suggest that electrified clouds also account for a significant, albeit relatively small component of the ionospheric variability.

© 2009 Elsevier Ltd. All rights reserved.

1. Introduction

An electrodynamic coupling between tropospheric thunderstorm generators and the ionosphere has been realized for nearly a century (Rodger, 1999) but there is still inadequate evidence revealing the causal pathways. Recent optical observations of 'sprites' initiated near the base of the ionosphere and the development of 'blue jets' propagating upwards from the top of thunderstorms (Pasko, 2007) combined with statistical evidence for enhanced electron concentrations in ionospheric sporadic-E (Es) layer associated with negative cloud-to-ground (CG) lightning strokes (Davis and Lo, 2008) have established an electrodynamic link between the troposphere, mesosphere, and ionosphere. Latest reviews of atmospheric electricity (Siingh et al., 2005; Rycroft, 2006) encourage researchers to identify the signatures of thunder-

storms on the F-region electric fields, as this is one of the least understood aspects of the global electrical circuit (Kartalev et al., 1998).

Conceptually, vertical mass exchange between the lower atmosphere and ionosphere is not plausible beyond 100 km, but electric fields are not bounded by these conditions (Rishbeth, 2006), as the ionosphere is not a perfect conductor. Several mechanisms help to mediate coupling between thunderstorms and the ionosphere: enhanced conductivity above thunderstorms (Rodger, 1999); quasi-electrostatic fields above thunderstorms, and associated heating of the lower ionosphere (Pasko et al., 1998); lightning associated AC phenomena (Rycroft, 2006), and wave dynamics including infrasonic and acoustic gravity waves (AGWs) (Johnson and Davis, 2006).

Previous work suggests that storm systems influence the F-region ionosphere through pressure changes and the AGWs they generate (e.g., Šauli and Boška, 2001), irrespective of the occurrence of lightning. It is important to note that whilst this paper identifies significant responses of the F-region ionosphere occurring in association with lightning, the lightning may or may not be the direct physical cause or trigger for the observed responses. The passage of thunderstorm cells is a complicated phenomena entailing many concurrent atmospheric processes (pressure fronts, intense winds, electrified clouds, lightning, etc.).

* Corresponding author. Tel.: +61 0 449751712, +61 0 400019618.

E-mail addresses: v.kumar@latrobe.edu.au (V.V. Kumar), m.parkinson@latrobe.edu.au (M.L. Parkinson), p.dyson@latrobe.edu.au (P.L. Dyson), Gary.Burns@aad.gov.au (G.B. Burns).¹ These authors contributed equally to this work.² Tel.: +61 3 9479 1433; fax: +61 3 9479 1552.³ Tel.: +61 9479 2735; fax: +61 3 9479 1552.⁴ Tel.: +61 3 62323381; fax: +61 3 62323496.

Lightning may be the cause or merely a proxy for the causes. Extremely comprehensive, multi-instrument studies of all the inter-connected atmospheric layers may ultimately be required to unambiguously identify the actual physical causes.

In this work, we use part of a 5.5-year (February 1999–August 2004) digital ionosonde (DPS-4) database compiled at a southern mid-latitude station, Bundoora, Melbourne (145.1°E, 37.7°S) (Kumar et al., 2008), 1-min auroral electrojet (AE) index and World Wide Lightning Location Network (WWLLN) (Dowden et al., 2002) data, to determine thunderstorm-associated responses in the overhead ionosphere. The chosen study interval was August 2003–2004, the first year WWLLN was fully operational. The DPS-4 measurements were also continuous during this 1-year interval.

The mid-latitude F-region is controlled by the E-(day) and F-(night) region dynamos during geomagnetically quiet times, and ionospheric disturbance dynamo and prompt penetration fields during disturbed times (Kumar et al., 2008 and references therein). In the method adopted here, the local time, seasonal, and magnetic activity-dependent average velocities were removed from the measurements. The residuals were then analysed with respect to the lightning times using a superposed epoch analysis (SEA). SEA has been frequently employed to identify relatively weak responses swamped by other competing influences operating over similar time scales (Prager and Hoenig, 1989; Davis and Lo, 2008).

In this paper, we report statistically significant, reproducible responses in the vertical motion of the F-region ionosphere associated with cloud-to-ground lightning strokes located within 600 km of Melbourne. Although these responses may be directly related to lightning, it is important to recall that lightning may be a proxy for some other atmospheric process. This paper concentrates on the analysis of the vertical velocity component because it is the most accurate velocity component measured by the digital ionosonde (Parkinson et al., 2001), and it readily reveals significant responses. However, preliminary analysis suggests small but significant responses in the horizontal motions which will be reported elsewhere.

2. Instruments and data analysis

2.1. F-region data

The Bundoora DPS-4 records ionograms by scanning between 2 and 12 MHz in steps of 100 kHz for less than 2-min, once every

10-min. During the intervening 8-min, Doppler sorted interferometry (DSI) (Parkinson et al., 1997) measurements were made using ordinary mode polarization at licensed fixed frequencies. A relatively small number of echoes with virtual heights below 180 km were classified as E-region data and excluded. The standard Digisonde Data Analysis (DDA) software was used to estimate 3D drift velocity in a Cartesian reference frame. The use of a long integration time (40.96-s) and thus high Doppler resolution meant that our estimates of vertical velocity V_z were very accurate (Parkinson et al., 2001). Kumar et al. (2008) analysed the entire DPS-4 F-region database and found that the velocities exhibited well-defined diurnal and seasonal variations with strong sensitivity to AE. The results were consistent with earlier studies using incoherent scatter radar (e.g. Buonsanto et al., 1993). Any relatively weak responses in the F-region drifts to electrified cloud activity may be masked by the normal Sq dynamo, the disturbance dynamo, and prompt penetration fields. We addressed this problem by creating a statistical model using the 5.5-year F-region database, with the results separated into two representative seasons, the spring–summer months (September–February) and autumn–winter months (March–August). Also, it was found the drift magnitudes were generally larger than usual in the year 2003 (Kumar et al., 2008) due to the high-speed solar wind streams known to re-occur during the declining phase of solar activity (e.g. Cliver et al., 1996). “DC offsets” associated with year-to-year variations were incorporated in the model.

The model, hereafter the *LT–AE model*, consisted of average velocity components calculated using 10-min bins in local time (LT) and 100 nT bins of the AE. The AE data of 1-min resolution was downloaded from the World Data Centre, Kyoto (<http://swdcwww.kugi.kyoto-u.ac.jp/aeasy/index.html>). An average velocity was calculated provided there were at least 500 samples per bin, thereby maintaining the statistical significance of the model. The upper limit for AE in the LT–AE model was 1000 nT. In situations when AE > 1000 nT, the model gives values corresponding to 1000 nT and the local time of measurement.

The validity of the LT–AE model was checked using all 31,376 drift velocities recorded during the interval August 2003–2004. The results for the vertical velocity V_z component are summarised in Fig. 1. Part (a) (top) shows the LT variation of raw V_z and indicates that the mean V_z (white curve) was strongly downwards up to 11 m s⁻¹ at dawn, reverting to gradually upwards up to 6 m s⁻¹ by dusk. The mean V_z was near to 0 m s⁻¹ in the post-midnight sector. Fig. 1a (bottom) shows the perturbations in

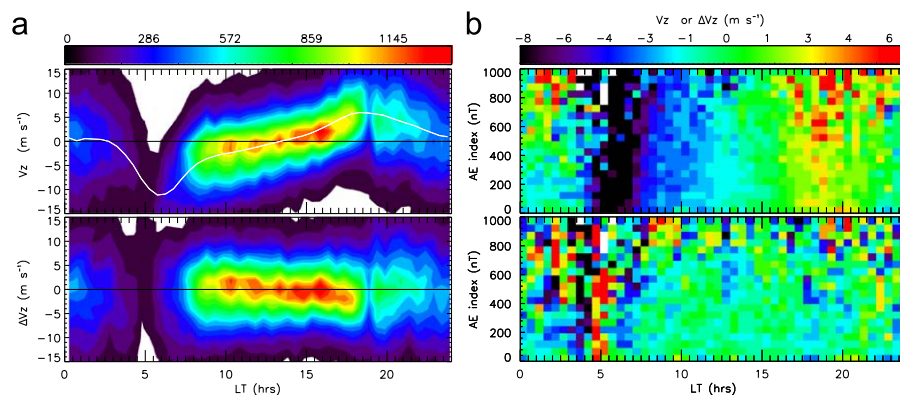


Fig. 1. Summary plots of the vertical velocity V_z and the perturbations in vertical velocity ΔV_z , with LT and AE for the interval August 2003–2004. ΔV_z is the residuals obtained by subtracting LT–AE model velocities from every raw V_z . (a) The diurnal variation of raw V_z (top) and of ΔV_z (bottom) using a bin size of 30-min in LT and 1 m s⁻¹ in V_z . The solid white curves are the average variations for each panel. (b) The diurnal variation of raw V_z (top) and of ΔV_z (bottom) with increasing AE, using a bin size of 50 nT.

vertical velocity ΔV_z , obtained by subtracting the LT–AE model from every raw V_z . Clearly, the residuals show a random distribution about the mean and the mean ΔV_z was almost 0 m s^{-1} at all local times. Although small negative values of ΔV_z occurred after 16 LT, it will be shown they cannot explain the much larger negative perturbations associated with lightning.

Likewise, Fig. 1b (top) is the response in raw V_z with increasing AE and indicates a net upward enhancement in V_z during the late afternoon and night whilst no significant change occurred during the daytime. Fig. 1d shows ΔV_z versus AE. The magnitude of residuals was larger during the morning and at higher AE values, but again the structure was removed. The results throughout Fig. 1b (bottom) confirm that the LT–AE model adequately eliminated the strong diurnal and AE dependence from the V_z component.

The residuals ΔV_z were used in a SEA analysis to investigate their response to electrified cloud activity. The point behind processing the V_z data in this way was to sensitise the SEA analysis to processes independent of solar zenith angle (LT) and geomagnetic activity. Although simply subtracting the monthly median values would be a legitimate alternative approach, it would not necessarily correct for perturbations associated with enhanced geomagnetic activity which varies in a complicated way with LT.

2.2. Electrified cloud activity

Lightning data obtained from WWLLN was used as a proxy for the intensity of electrified cloud activity. CG lightning discharges emit very low frequency (VLF) radiowave pulses, ‘sferics’, with peak emission at $\sim 10 \text{ kHz}$. The radiated pulse propagates with little attenuation in the Earth–ionosphere waveguide. WWLLN employs the Time of Group Arrival (TOGA) of the VLF radiation to locate the position of the strokes. TOGA is obtained to μs accuracy, giving positional errors as low as 2 km (Dowden et al., 2002). Comparative study of lightning strokes detected by WWLLN and other lightning detection networks revealed that WWLLN was sensitised to discharge currents $> 70 \text{ kA}$, whilst other system have a lower threshold of 20 kA (Ramachandran et al., 2005).

The horizontal extent of the vertical thunderstorm–ionosphere coupling can range between ~ 30 and 300 km (Tonev and Velinov, 2007) and may last for up to few hours. Roble and Tzur (1986) simulated electrostatic potential contours above the thunderhead extending to ionospheric heights and predicted that the width of the coupling decreases with increasing magnetic latitude because of the steeper inclination of the magnetic field. Initially, our analysis used all lightning data within a 200 km radius of the Bundoora DPS-4, comparable to the limits employed elsewhere (Johnson and Davis, 2006; Davis and Lo, 2008). The main result to be shown in Fig. 3 was obtained, but the responses were statistically less significant due to fewer events (1457 strokes). Thus, the threshold radius for selecting the lightning strokes was increased.

All lightning strokes detected within a 600 km radius of the Bundoora DPS-4 were used in this study as a compromise between the need to increase the statistical significance of results whilst ensuring the observed responses were related to local thunderstorm activity. In total, 24,202 lightning strokes were detected by an average of 5 WWLLN stations and these lightning times were used as the “controls” ($t = 0$) for in SEA of F-region Doppler shift data. Because most of the lightning occurred far away, the F-region responses reported here probably represent lower limits to the actual responses occurring directly above thunderstorms.

CG flash densities as function of radial distance were calculated to confirm that lightning strokes at radius 600 km belonged to the same thunderstorm system passing nearby Bundoora.

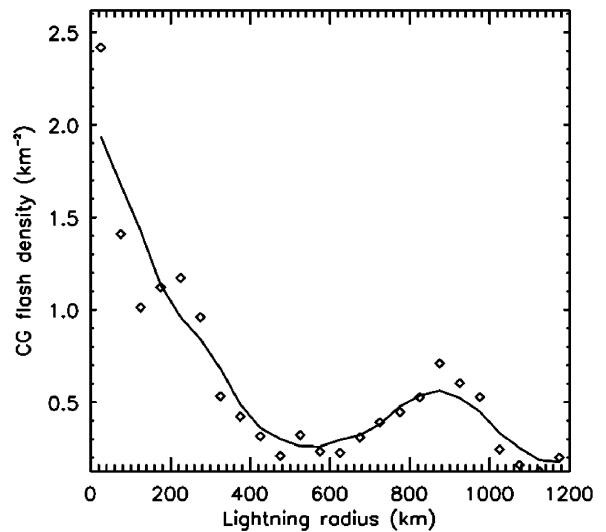


Fig. 2. CG flash densities versus increasing radial distance from Bundoora, Victoria. The data used for this plot is explained in the text. The solid curve is a 5-point running average.

For every lightning stroke occurring within 200 km of Bundoora, all the lightning strokes detected within $\pm 6 \text{ h}$ were used to estimate the flash density in circular regions with radius increasing by steps of 50 km out to a maximum radius of 1200 km. The results are shown in Fig. 2 and suggest a characteristic scale of $\sim 850 \text{ km}$ separating the occurrence of separate thunderstorm systems. Thus, lightning occurring within a $\sim 600 \text{ km}$ radius can be thought of as belonging to the same local thunderstorm system.

3. Results

Fig. 3 shows a SEA of perturbations in the vertical drift velocity (ΔV_z) of the mid-latitude F-region ionosphere in response to CG lightning strokes for three different datasets, “Sets 1, 2, and 3” (to be defined). The results for Sets 1–3 are shown using red, dotted black and solid black curves, respectively. Consistent with the LT–AE model, a bin size of 10-min was used for all estimates of averages and standard deviations of the mean.

“Set 1” used all the CG lightning and F-region data within 48 h on either side of each lightning stroke that occurred within a circular region of radius 600 km relative to Bundoora. Fig. 3a shows the Set 1 results for CG lightning counts (red curve) plotted on a logarithmic scale. As expected, the distribution is symmetric about $t = 0$. There is also evidence for periodicity in the curve related to the daily re-occurrence of thunderstorms, with peak activity concentrated near 3 pm LT.

In contrast, “Set 2” provides an estimate of the variation in ΔV_z expected when electrified cloud activity was relatively weak or absent. Set 2 was analysed in the same way as Set 1 except it only used velocities contained within the time windows (-144 to -96) and (96 – 144) h, chosen because they correspond to troughs in the lightning occurrence. In addition, any data recorded on lightning active days were excluded. A nominal threshold of > 30 strokes-per-day within 200 km effectively separated the lightning active days from a general background of sporadic discharges.

The SEA analysis of Set 2 was based upon the same lightning times as Set 1 (red curve), but the SEA of lightning for Set 2 (Fig. 3a, dotted curve) was calculated by mapping $\pm 96 \text{ h}$ to $t = 0$, thereby preserving the local time variation. As shown, the lightning activity was reduced by more than an order of

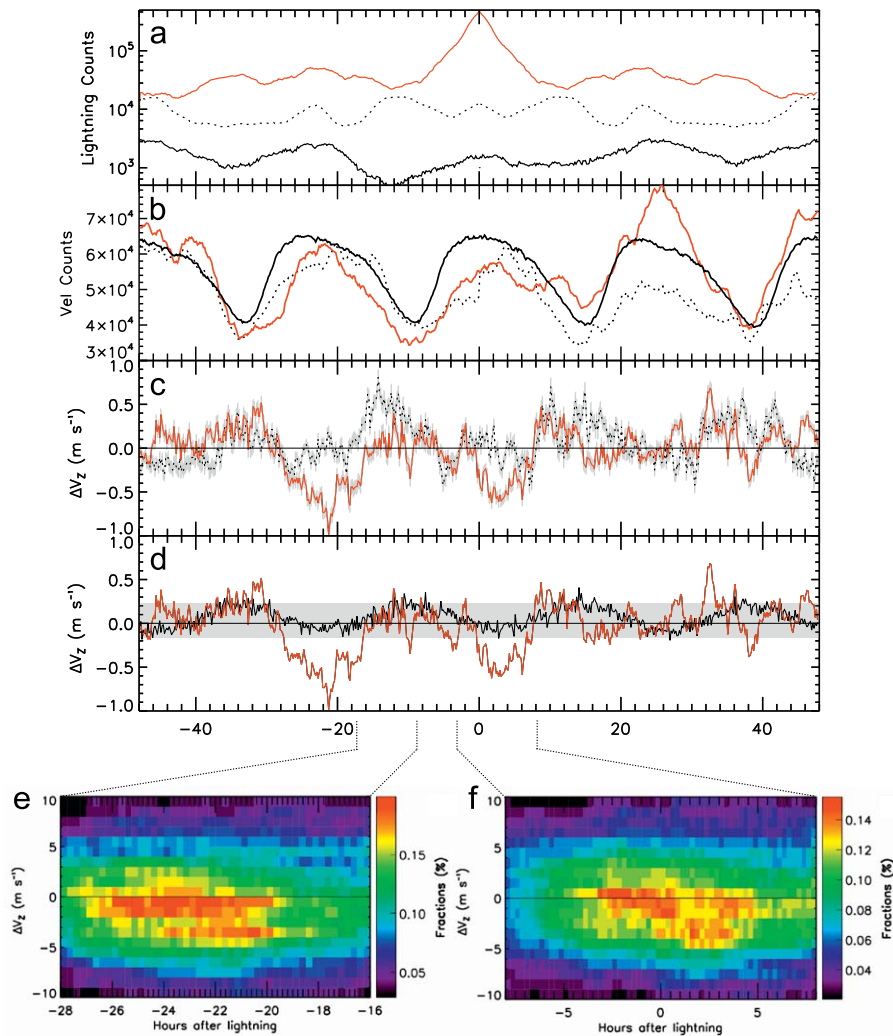


Fig. 3. Superposed epoch analyses (SEA) of the perturbations in the F-region vertical velocity ΔV_z using CG lightning strokes as controls ($t = 0$) “Set 1” (red curves). As explained in the text, SEA results are also shown for two other datasets “Set 2” (dotted black) and “Set 3” (solid black) providing alternative estimates of the responses expected in the absence of electrified clouds. A bin size of 10-min was used in this figure. (a) SEA of the CG lightning counts for the three data sets. (b) Same as (a) except for the F-region velocity counts. (c) SEA of the average perturbation in the vertical velocity, ΔV_z , for Sets 1 and 2. A positive ΔV_z represents a net upward motion of the ionosphere. The gray-shaded region around each curve is the standard errors of the means; repetitive data samples within each 10-min bin were excluded. (d) Same as (c) except for Sets 1 and 3. The 2σ level of the fluctuation in ΔV_z for Set 3 is 0.23 m s^{-1} and is indicated by the horizontal shaded region. (e) The distribution of ΔV_z values between -28 and -16 h calculated using a bin size of 1 m s^{-1} in ΔV_z . The fraction in % was calculated from the ratio of the number of ΔV_z values in each bin to the total number of ΔV_z values from -28 to -16 h. (f) Same as e except for the SEA times of -8 to $+8$ h. (For interpretation of the references to colour in this figure legend, the reader is referred to the web version of this article.)

magnitude at $t = 0$, but there was nearly always a weak background of lightning, and it is nearly impossible to define an expected variation completely free of electrical activity.

“Set 3” provides an improved estimate of the variations expected in the absence of electrified cloud activity. Instead of using real lightning times, 24,202 (equal in size to the real lightning times) synthetic lightning times were generated using identical times of day as the real lightning times, but with the day numbers generated using an ideal random number generator. Again, synthetic day numbers which overlapped with nominally lightning active days were excluded. The asymmetry in Set 3 (Fig. 3a solid black) was caused by a separate set of synthetic controls times probing the real lightning times. At all times, the SEA of lightning counts for Set 3 was at least an order of magnitude less than for Set 1.

Fig. 3b shows the SEA of F-region velocity counts per 10-min bin for the three datasets. A more detailed summary of the velocity counts for Sets 1–3 is given in Fig. 4a–c, respectively.

Fig. 4 uses a bin size of 10-min in lightning time and 1 h in LT. The upward sloping striations in Fig. 4 arise from the passage of discrete thunderstorm cells (lightning clusters) throughout the study interval. The main point behind showing Figs. 3b and 4 is to demonstrate the subsequent SEA analysis of the V_z component is based upon tens of thousand of real and synthetic lightning strokes selecting many thousands of statistically independent velocities per 10-min bin. Fig. 4 also confirms that the LT bias in the number of SEA samples for all datasets are similar and thus any artefacts created by the LT–AE model will be similar. In summary, the statistical significance of the main result presented in Fig. 3c and d is beyond doubt.

For DSI, the number of velocities and their accuracy tends to increase with ionospheric roughness (Parkinson et al., 2001). However, other factors affect the number of estimated velocities including electrical interference, ionospheric absorption, and the difference between the transmission frequency and $f_o F_2$, all of which can lead to poor signal-to-noise ratio (SNR). For the entire

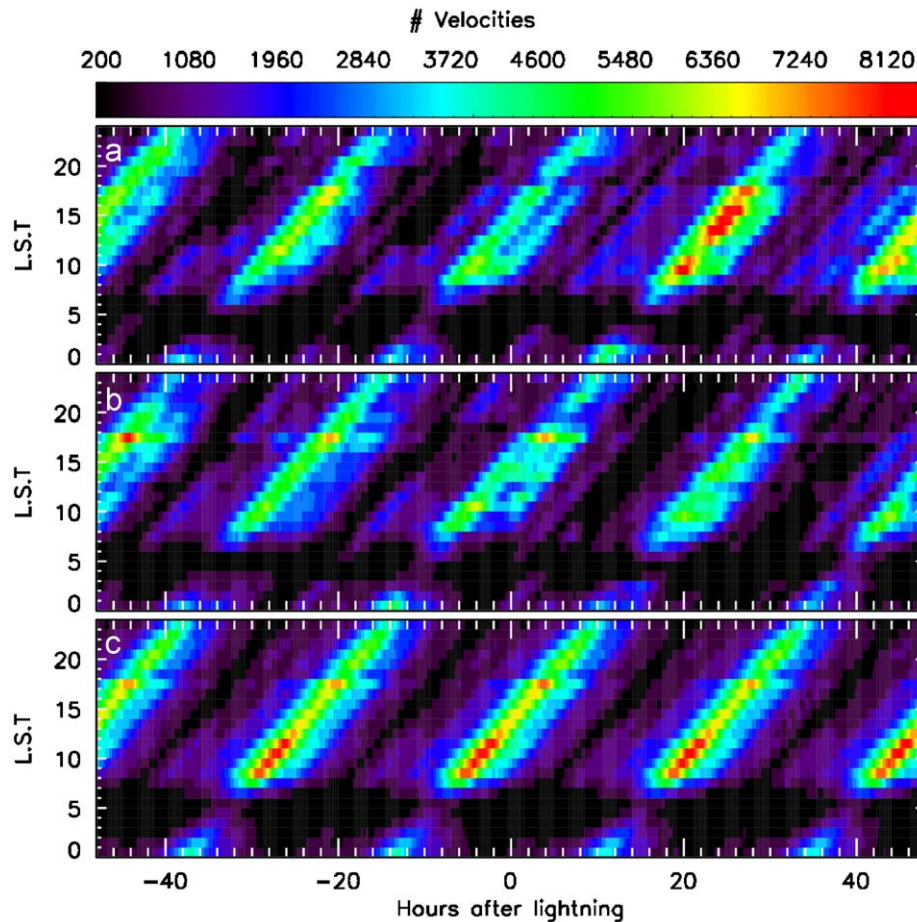


Fig. 4. Colour map showing the temporal variation of the number of F-region velocities in (a) Set 1, (b) Set 2, and (c) Set 3. The velocities were counted using bin sizes of 10-min bin in lightning time and 1 h bin in LST. (For interpretation of the references to colour in this figure legend, the reader is referred to the web version of this article.)

5.5-year database, the number of velocities tended to be higher during the daytime (as shown in Fig. 4) and up to 20% greater during geomagnetic disturbances.

At face value, the results shown in Figs. 3b and 4a suggest the velocity counts were suppressed before and on the day of thunderstorms, and enhanced on the day after. Clearly, this feature is absent within the time windows (−144 to −96) and (96–144) h (Fig. 4b) and with synthetic lightning times (Fig. 4c). However, variability in the SNR and the particular sequence of geomagnetic storms occurring during the study interval negate any relationship between lightning and ionospheric roughness. The LT–AE model was not used to correct the velocities counts. Such a model would only be partly successful because of the various factors affecting the velocity counts.

Fig. 3c and d shows the SEA results for mean ΔV_z for the three sets and they were separated into two panels for clarity. Extreme outliers beyond the range $\pm 10 \text{ m s}^{-1}$ in ΔV_z ($< 4.2\%$ of samples) were rejected prior to averaging. The gray shading around each curve in Fig. 3c was formed by the envelope of standard errors of the mean, σ/\sqrt{n} where σ is the standard deviation and n is the number of samples. Repetitive samples within each 10-min bin did not contribute to n . Likewise, the shaded region in Fig. 3d represents the 2σ level of 0.23 m s^{-1} for residual fluctuations in ΔV_z for the synthetic data, Set 3. An ionospheric response was considered significant if its amplitude consistently exceeded the $\pm 2\sigma$ level of the null hypothesis curves.

The Set 2 (dotted curve) and Set 3 results (solid black curves) in Fig. 3c and d, respectively, are very similar in that the Set 3 results

are essentially a low pass filtered version of the Set 2 results. In contrast, the Set 1 results (red curve) show distinct downward perturbations in V_z between −27 and −16 h before lightning and between 0 and 6 h after lightning. Interestingly, the two regions of distinct downward enhancements, relative to the two black curves, were separated by ~ 24 h, with the dominant peak occurring at ~ -21 h (the day before). However, this does not violate causality because the lightning times were merely a proxy for the atmospheric processes involved.

Fig. 1a (bottom) showed that after using the LT–AE model to correct the V_z values, small negative values of ΔV_z occurred after 16 LT. Fig. 3c and d show small negative perturbations in ΔV_z for Sets 2 and 3 coincident with the much larger negative perturbations for Set 1, the SEA results using real lightning times. The small negative perturbations in ΔV_z for Sets 2 and 3 partly arise because the LT–AE model was imperfect. However, they do not explain the much larger negative perturbations in ΔV_z found for Set 1 because all three sets share a similar LT bias of lightning times (Fig. 4), yet the negative perturbations for Set 1 were separated by well over 2σ from the results for Sets 2 and 3. Moreover, an examination of uncorrected time series of V_z often revealed swings to negative values during the afternoon of thunderstorm days, a time of day when the ionosphere would normally be ascending.

Fig. 3c and d gave the mean variation per 10-min bin, but they did not reveal the distribution of velocities contributing to the means. Fig. 3e and f show the distribution of the numbers of ΔV_z values during the intervals when the negative perturbations were most pronounced. The plots clearly indicate the negative

perturbations were the net effect of a large number of small events, up to -4.5 m s^{-1} . Only a few short-lived variations, such as the negative spike located at $\sim -21 \text{ h}$, were due to a few dominant events.

Finally, many features outside the time windows -27 to -16 h before lightning and 0 to 6 h after lightning were not well separated from the gray curves and are statistically insignificant, and some of the responses at longer delays were residuals due to the LT–AE model failing to represent the actual LT variations within the study interval.

4. Discussion and summary

Fig. 3c–f showed the main result of this paper, namely the gradual negative perturbations in ΔV_z at ~ -21 and $\sim +3 \text{ h}$ for data Set 1. These perturbations were real, statistically significant features because (1) they were often recognised in individual case study data (not shown), (2) the statistical results shown in Fig. 3 were based upon many thousands of independent samples, (3) the LT–AE model generates residuals in LT with the magnitude of ΔV_z generally less than 0.23 m s^{-1} , and always less than the amplitude of the two main negative perturbations, (4) There was no evidence for these perturbations in the null hypothesis test results, Sets 2 and 3, and (5) the standard error bars indicate that the peaks at ~ -21 and $\sim +3 \text{ h}$ in Set 1 are statistically significant with respect to Set 2 at the 97.47% and 97.22% levels, and with respect to Set 3 at the 99.94% and 99.68% levels, respectively.

It is generally argued that slowly varying (DC) electric fields will not penetrate far into the highly conducting ionosphere and thus other theory must be considered to explain the observed gradual negative enhancements in ΔV_z . The following qualitative conjecture discusses the likelihood of three plausible explanations. However, more observations and theory will be required to unravel the physical processes involved.

1. Electrical energy deposited during upward lightning discharge cause ionisation enhancements in the lower ionosphere, via ionisation created by direct breakdown of neutrals (Taranenko et al., 1993) and particle precipitation induced by wave–particle interactions (Strangeways, 1999). Production of ionisation at lower altitudes is equivalent to a descending ionosphere from the point of view of Doppler shift, analogous to the sunrise effect. The peak responses in V_z were delayed by $\sim 3 \text{ h}$, longer than expected for the immediate effects of lightning and the subsequent decay of ionisation via recombination. However, the delay may result from the accumulative effect of numerous lightning discharges.
2. Modelling of large-scale electrical activity associated with tropospheric thunderstorms (Roble and Tzur, 1986) reveal significant gradients of electric potential penetrating into the E-region ionosphere, and thus ultimately the F-region. Horizontal DC electric fields of the order of 100 mV m^{-1} were measured in the mesosphere above a moderate mid-latitude thunder-cell (Holzworth et al., 1985). These were over an order of magnitude larger than electric fields expected during fair weather. Significant Doppler shifts will be observed if only 1% of these fields penetrate the ionosphere. For regions of large magnetic dip angles such as Bundoora (-69°), vertical electric field coupling above localised thunderstorms will penetrate to greater altitudes in the ionosphere (Roble and Tzur, 1986).
3. An AGW with phase speed 55 m s^{-1} can, in principle, travel $\sim 600 \text{ km}$ in 3 h . The upward propagating AGWs break in the lower thermosphere and transfer momentum to the mean neutral flow (Medeiros et al., 2004). The modified winds will

generate electric fields via dynamo action and then perturb the F-region ionosphere.

There is ambiguity between explanations (2) and (3), because the ionised and neutral atmospheres are coupled via collisions. In (2) the electric fields penetrating into the bottom side ionosphere gradually accelerate the collision-dominated ions and thus neutrals via ion drag (e.g. Kelley, 1989). In turn this will generate dynamo fields which feed back upon the F-region ion flow. In (3) the AGWs will modify the E-region neutral winds and thus generate dynamo electric fields. It is well known that the motion of the ionised and neutral atmospheres will reach a new “equilibrium” in the order of $\sim 2\text{--}3 \text{ h}$, close to the time delay observed for our negative perturbations in V_z .

On the other hand, larger downward responses in V_z on the day before (and the weaker responses on the day after) are consistent with causality because the lightning strokes were merely proxies for the physical processes involved. Although only a working hypothesis, the asymmetry in the observed responses may be related to local meteorological conditions. The WWLLN data indicated that thunderstorms above Bundoora occurred in a runs of 2–3 days. The strongest electrical activity tended to occur on the first day and then gradually decay to the least on the last day. The gradual decline in the response from one day to the next is consistent with the notion that electrified clouds generate potential difference in competition with subsequent discharge by lightning (Singh et al., 2005).

The lightning occurring above Melbourne was often associated with low-pressure troughs or cells preceded by cold fronts which typically approached the station from the Great Australian Bite located $\sim 1000 \text{ km}$ west of the station. A further analysis of lighting occurrence within 1200 km of Bundoora confirmed the strokes were concentrated to the west of station on the day before. The lightning counts were similar to the values measured when thunderstorms passed nearby the station, yet $\sim 40\%$ larger than on the day after (i.e. a decay in the energy release).

AGWs are known to be generated by thunderstorms (Medeiros et al., 2004) and sprites (Sentman et al., 2003), but they are also generated by strong atmospheric fronts irrespective of lightning (Šauli and Boška, 2001). Thus, it would be worthwhile to search for similar signatures in V_z during the passage of electrically inactive cold fronts passing across the station to help clarify the role of lightning. This worthy study is beyond the scope of the present paper.

The relative importance of the various mechanisms is not clear and the effects of lightning on the Earth’s radiation belts may also play a role. Many more studies of this kind are needed to better understand the responses and clarify the physical mechanisms involved.

Acknowledgements

This work was supported by an internal research grant awarded by the La Trobe University. We thank the WWLLN for providing lightning data over the region. The financial support for Vickal V. Kumar was provided by an Australian Government Endeavour Postgraduate Award (ESPA_DCD_365_2007).

References

- Buonsanto, M.J., Hagan, M.E., Salah, J.E., Fejer, B.G., 1993. Solar cycle and seasonal variations in F region electrodynamics at Millstone hill. *Journal of Geophysical Research* 98, 15677–15683.
- Cliver, E.W., Boriakoff, V., Bounar, K.H., 1996. The 22-year cycle of geomagnetic and solar wind activity. *Journal of Geophysical Research* 101, 27091–27109.

- Davis, C.J., Lo, K., 2008. An enhancement of ionospheric sporadic-E layer in response to negative polarity cloud-to-ground lightning. *Geophysical Research Letters* 35.
- Dowden, R.L., Brundell, J.B., Rodger, C.J., 2002. VLF lightning location by time of group arrival, TOGA at multiple sites. *Journal of Atmospheric and Solar-Terrestrial Physics* 64, 817–830.
- Holzworth, R.H., Kelley, M.C., Siefring, C.L., Hale, L.C., Mitchell, J.D., 1985. Electrical measurements in the atmosphere and the ionosphere over an active thunderstorm 2 Direct current electric fields and conductivity. *Journal of Geophysical Research* 90, 9824–9830.
- Johnson, C.G., Davis, C.J., 2006. The location of lightning affecting the ionospheric sporadic-E layer as evidence for multiple enhancement mechanisms. *Geophysical Research Letters* 33, L07811.
- Kartalev, M.D., Rycroft, M.J., Papitashvili, V.O., 1998. A quantitative model of the effects of global thunderstorms on the global distribution of ionospheric electrostatic potential. *Journal of Atmospheric and Solar-Terrestrial Physics* 66, 1233–1240.
- Kelley, M.C., 1989. *The Earth's Ionosphere*. Academic Press, California.
- Kumar, V.V., Parkinson, M.L., Dyson, P.L., Polglase, R., 2008. Solar and geomagnetic effects on mid-latitude F-region plasma electric field. *Annales Geophysicae* 26, 2911–2921.
- Medeiros, A.F., Takashi, H., Batista, P.P., Gobbi, D., Taylor, M.J., 2004. Observation of atmospheric gravity waves using airglow all-sky CCD imager at Cachoeira Paulista, Brazil (23°S, 45°W). *Geofisica Internacional* 43 (1), 29–39.
- Parkinson, M.L., Dyson, P.L., Smith, P.R., 1997. Analysis of direction-of-arrival aliasing for MF/HF Doppler-sorted interferometry measurements of ionospheric drift. *Radio Science* 32 (3), 999–1009.
- Parkinson, M.L., Polglase, R., Fejer, B.G., Scherliess, L., Dyson, P.L., Ujmaia, S.M., 2001. Seasonal and magnetic activity variations of ionospheric electric fields above the southern mid-latitude station, Bundoora, Australia. *Annales Geophysicae* 19, 521–532.
- Pasko, V.P., 2007. Red sprite discharge in the atmosphere at high altitude: the molecular physics and the similarity with laboratory discharge. *Plasma Sources Science and Technology* 16, S13–S29.
- Pasko, V.P., Inan, U.S., Bell, T.F., 1998. Ionospheric effects to electrostatic thundercloud fields. *Journal of Atmospheric and Solar-Terrestrial Physics* 60, 863–870.
- Prager, M.H., Hoenig, J.M., 1989. Superposed Epoch Analysis: a randomization test of environment effects on recruitment with application on chub mackerel. *Transactions of the American Fisheries Society* 118, 608–618.
- Ramachandran, V., Kumar, S., Kishore, A., 2005. Remote sensing of cloud-to-ground lightning location using the TOGA of sferics. *Atmospheric Science Letters* 6, 128–132.
- Rishbeth, H., 2006. F-region links with the lower atmosphere. *Journal of Atmospheric and Solar-Terrestrial Physics* 68, 469–478.
- Roble, R.G., Tzur, I., 1986. The global atmospheric electrical circuit. In *Study in geophysics—the earth's electrical environment*. National Academy of Science Washington DC, 206–231.
- Rodger, C.J., 1999. Red sprites, upward lightning, and VLF perturbations. *Reviews of Geophysics* 37 (3), 317–336.
- Rycroft, M.J., 2006. Electrical processes coupling the atmosphere and ionosphere: an overview. *Journal of Atmospheric and Solar-Terrestrial Physics* 68, 445–456.
- Šauli, P., Boška, J., 2001. Tropospheric events and possible related gravity wave activity effects on the ionosphere. *Journal of Atmospheric and Solar-Terrestrial Physics* 63 (9), 945–950.
- Sentman, D.D., Wescott, E.M., Picard, R.H., et al., 2003. Simultaneous observations of mesospheric gravity waves and sprites generated by a midwestern thunderstorm. *Journal of Atmospheric and Solar-Terrestrial Physics* 65 (5), 537–550.
- Siingh, D., Singh, R.P., Kamra, A.K., Gupta, P.N., Singh, R., Gopalakrishnan, V., Singh, A.K., 2005. Review of electromagnetic coupling between the Earth's atmosphere and the space environment. *Journal of Atmospheric and Solar-Terrestrial Physics* 67, 637–658.
- Strangeways, H.J., 1999. Lightning induced enhancements of D-region ionisation and whistler ducts. *Journal of Atmospheric and Solar-Terrestrial Physics* 61, 1067–1080.
- Taranenko, Y.N., Inan, U.S., Bell, T.F., 1993. Interaction with the lower ionosphere of electromagnetic pulses from lightning: heating, attachment, and ionization. *Geophysical Research Letters* 20 (15), 1539–1542.
- Tonev, P.T., Velinov, P.I.Y., 2007. Atmosphere—ionosphere vertical electric coupling above thunderstorms of different intensity. *Journal of Atmospheric and Solar-Terrestrial Physics* 69, 2510–2522.